Journal of Analytical Science and Technology

RESEARCH ARTICLE Open Access

Nano-fluorescent quantum dots as substrates for determination of ribavirin in pharmaceuticals and human plasma as well as monitoring of its kinetic interaction with salmon sperm DNA

Ahmed Faried Abdel Hakiem[1*], John M. Boushra[2], Deena A. M. Noureldeen[3], Adel S. Lashien[2] and Tamer Z. Attia[3]

Abstract

Ribavirin (RIB) was successfully determined by fluorescence spectroscopy upon its quenching to environment friendly phosphorus and nitrogen co-doped carbon quantum dots (PNQDs). Different analytical parameters affecting the fluorescence spectra have been optimized and validated in accordance to the ICH guidelines. The proposed method has provided an efficient tracing of the interaction between RIB molecules and the synthesized QDs in an acidic medium (off-mode). The RIB molecules have shown excellent sensitivity by quenching of the emission band at 401 nm upon excitation at 245 nm throughout a linear range of 0.06–10.00 µg/mL with detection and quantitation limits down to 14.00 and 40.00 ng/mL, respectively. The quenching mode was proven to be static in raw samples and samples extracted of spiked plasma for quenching rate constants of 1.30×10^{12} L M^{-1} S^{-1} and 1.73×10^{12} L M^{-1} S^{-1}, respectively. The proposed method has been successfully applied for determination of RIB in the commercial capsules and spiked human plasma samples with good recovery percentages in between 102.00 and 103.00%. Interestingly, these carbon dots have been utilized as nano-fluorescent platforms for assessment of the binding interaction kinetics between the RIB molecules and salmon sperm DNA (ssDNA). This has been implemented through peeling off the RIB molecules from surface of the PNQDs upon successive addition of the ssDNA and hence fluorescence restoration (turning on). Consequently, this provides a successful monitoring of its antimicrobial potency. It was evidenced a strong binding interaction with a binding constant of 2.38×10^{4} mol^{-1}/L. Significantly, this could open doors for an extended application for on-site monitoring of RIB as well as its interactions with biomolecules and microorganisms.

Keywords Flourescence spectroscopy, Determination of ribavirin, Phosphorus and nitrogen co-doped carbon quantum dots, Turning off (quenching) and turning on (peeling off), Commercial capsules and spiked human plasma, Binding interaction kinetics to ssDNA

*Correspondence:
Ahmed Faried Abdel Hakiem
ahmed_faried@pharm.kfs.edu.eg
Full list of author information is available at the end of the article

Introduction

Ribavirin is a synthetic guanosine analog nucleoside of broad-spectrum virustatic activity. Chemically, it is (1-(3,4-dihydroxy-5-hydroxymethyl-tetrahydrofuran-2-yl)-1H- (Snell 2001; Laurent and Shapiro 2006; Ali et al. 2020)-triazole-3-carboxylic acid amide), Fig. 1. It acts against DNA viruses like herpes simplex, cytomegalovirus and adenoviruses. It is considered a broad-spectrum antiviral agent as it acts also against RNA viruses including influenza, paramyxoviruses, respiratory syncytial virus and hepatitis C virus (Snell 2001; Laurent and Shapiro 2006; Thomas et al. 2012). It has been evidenced that it reduces the recovery period of COVID-19 patients treated with corticosteroids as well as inhibits the viral replication in combination with interferon β (Ali et al. 2020; Hung et al. 2020).

Nowadays, the carbon quantum dots (QDs) have gained much interest in the bioimaging and analytical applications. They are two-dimensional thick carbon nanoparticles with sp2 hybridization and physical dimensions less than the exciton Bohr radius (2.00–10.00 nm) exhibiting unique electronic and thermal criteria (Benítez-Martínez and Valcárcel 2015; Badıllı et al. 2020). They are synthesized by the surface passivation utilizing different routes (Singh et al. 2021). It has been proven that the QDs afford excellent optical merits of light stability, high quantum yield luminescence and resistance to photo-bleaching (Pan et al. 2020; Mahmoud et al. 2019; Alhazzani et al. 2023; Alqahtani et al. 2023; Mohamed et al. 2023).

Few analytical techniques had been previously reported for determination of RIB, mainly the RP-LC using UV detection in whole blood samples (Homma et al. 1999), simultaneously with α2-interferon in human serum (Larrat et al. 2003), simultaneously with sofosbuvir and daclatasvir in human plasma (Youssef et al. 2019) and in tablets (Wadie et al. 2017). Other RP-LC methods have utilized mass detection for determination of RIB in rat plasma (Zhang et al. 2016) and simultaneously with sofosbuvir, ledipasvir and silymarin in biological samples (El-Yazbi et al. 2021). Capillary electrophoresis–UV detection has been utilized for assessment of RIB in human serum and plasma samples (Breadmore et al. 2004). Ribavirin was analyzed simultaneously with sofosbuvir and saxagliptin by densitometric determination (El-Shaboury et al. 2018). Additionally, the pure form of RIB was quantified by UV-spectrophotometry (Kienskaya et al. 2019).

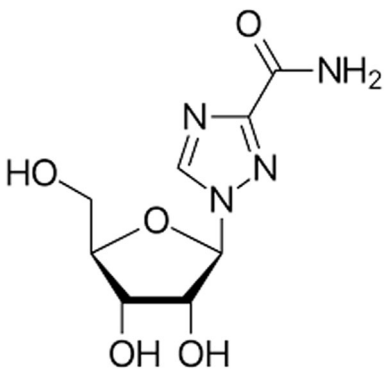

Fig. 1 The chemical structure of ribavirin

To the best of our knowledge, monitoring of the degree of binding to the nucleic acid gives an indication about the antiviral activity. Hence, the interaction of RIB with the calf-thymus DNA has been extensively investigated as wide theoretical modeling study (Vîjan and Topală 2016) and experimentally, by different spectroscopic techniques (Shahabadi et al. 2012). To date, the conjugation of ssDNA with RIB has not been monitored yet to investigate new eras of the therapeutic effects of RIB.

Comparatively to the previously reported liquid chromatographic methods with either DAD or mass detection, it provides greenness as it ensures the safety of personnel and environment by decreasing the use of carcinogenic solvents or by replacing them for more eco-friendly alternatives. Additionally, it is much more superior to these techniques with respect time consumption, cost effectiveness and simplicity, in Additional file 1: Table S1.

This research has afforded for the first time the synthesized eco-friendly carbon QDs derived from orange juice doped with phosphorus and nitrogen as a fluorescent facility for determination of RIB as well as its interaction with the ssDNA. The carbon quantum dots as luminescent platforms have introduced the potential merits of spectrofluorimetry as a fast, simple and highly sensitive technique (Franca and Nollet 2017), in the determination of the non-fluorescent RIB molecule as well as monitoring of its binding to the ssDNA.

In the present work, the conjugation of RIB with PNQDs in the proposed method has resulted in significant fluorescence quenching (turning off) providing superior sensitive way for determination of RIB in pharmaceuticals and human plasma samples. On the other hand, the competitive interaction of RIB and PNQDs with ssDNA was utilized for precise and sensitive assessment of the RIB–ssDNA interaction through restoring the fluorescence intensity (turning on).

Experimental

Materials

Ribavirin was kindly gifted from GLOBAL NAPI Pharmaceuticals (Giza, Egypt). The Salmon sperm DNA was

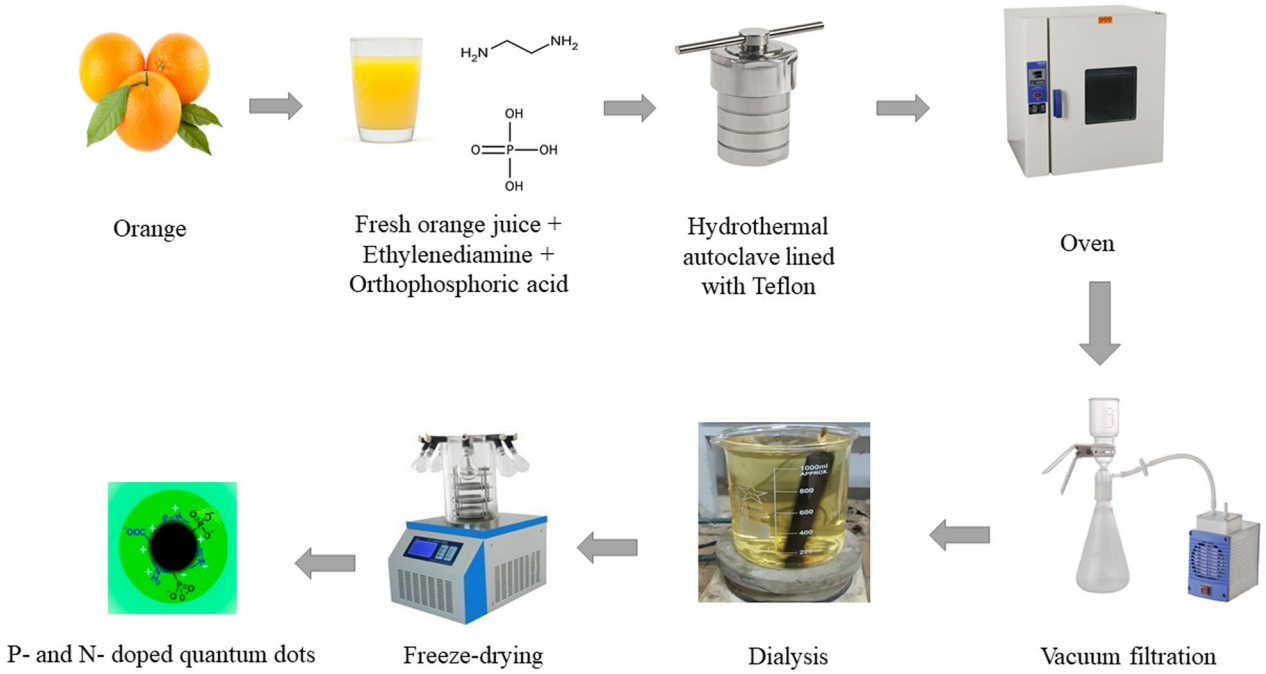

Scheme 1 Synthesis of the PNQDs

obtained from Sigma-Aldrich (St. Louis, USA). Tris–HCl (≥ 99%) and ethylenediamine (99%) were purchased from Merck KGaA (Darmstadt, Germany). Orthophosphoric acid (99.8%), sodium hydroxide (97.5%), potassium dihydrogen phosphate (99.9%) and potassium bromide (98.5%) were purchased from the El-Nasr Company for Pharmaceutical Chemicals (Abozabaal, Egypt). The plasma samples were provided by the National Egyptian Blood Bank and stored at − 20 °C until used.

Instrumentation

Luminescence spectrometer (PerkinElmer, UK) model LS 45, supplied with a 150 Watt xenon arc lamp, grating monochromators were set at 10 nm for excitation and emission using 1 cm quartz cuvette. The spectrometer was controlled with FL Winlab™ application software. Double beam UV–Visible spectrophotometer (Shimadzu, Japan) model UV-1601 PC with quartz cell of 1 cm path length and UV-PC personal software version 3.7. The spectral band width is 2 nm with wavelength scanning speed of 2800 nm/min. Teflon lined hydrothermal autoclave of 100.00 mL volume designed and manufactured locally according to the standard dimensions. A Nicollet IS 10 spectrometer (Thermo-Scientific Instruments Corp., Madison, WI USA) was utilized for FTIR investigations supported with OMNIC software for data processing in the range 4000–400 cm^{-1}. A Thermo-Scientific (Fischer, USA) Qwik handi-press instrument was exploited to compress the IR samples. Zeta analyzer (Malvern Zetasizer Nano-ZS90, Malvern Instruments Ltd., Malvern, U.K.). Digital analytical balance (AG 29, Mettler Toledo, Glattbrugg, Switzerland).

Synthesis of PNQDs

The quantum dots have been synthesized according to previous report (Parvin and Mandal 2017) with slight modifications. About 3.00 mL orthophosphoric acid, 0.30 mL ethylenediamine (slow and careful dropwise addition) and 54.00 mL pulp free orange juice purchased from the local market were introduced into the Teflon lined hydrothermal autoclave. The mixture was then heated in an electric oven at 190 °C for 12 h and allowed to cool at room temperature. The obtained brownish black solution was centrifuged at 3000 rpm for 20 min. The supernatant was subjected to suction filtration through 0.22 membrane filter. The filtrate was provided into dialysis membrane connected to magnetic bar and allowed to stir in one liter deionized water for 24 h, and water has been exchanged every one hour till obtaining clear and colorless solution. Finally, the solution was lyophilized to get solid dark brown carbon quantum dots, in Scheme 1.

Characterization of the obtained PNQDs

The synthesized quantum dots have been characterized by different techniques: Fourier-transform infrared (FTIR), transmission electron microscopy (TEM) and X-ray powder diffraction (XRPD). The FTIR spectrum has exhibited two bands at 3382 and 3225 cm^{-1} that correspond to the NH_2 stretching of a primary amine and the broadening is due to the hydrogen bonding which overlaps the stretching vibration of the hydroxyl moieties. The vibrational band at 2916 cm^{-1} is attributed to the CH_3 stretching. The vibrational features at 1635 and 1554 cm^{-1} represent the carbonyl of the carboxylate moiety and the hydroxyl bending, respectively. The band at 1435 cm^{-1} is attributed to a P–C stretching (symmetric deformation), while that at 1338 cm^{-1} represents the C–H bending vibration. The vibrational band at 1038 cm^{-1} is corresponding to the P–O stretching followed by a bending band of the O–H moiety presented at 929 cm^{-1} (Hakiem et al. 2020, 2021; Ali et al. 2020), in Fig. 2**.**

The morphology of the synthesized PNQDs has been displayed by the transmission electron microscope (TEM). The PNQDs are well dispersed and have shown almost typically spherical particles with a narrow particle size distribution mainly located in the range 3.68–6.52 nm with an average diameter of 4.78 nm. A small percentage not more than 7.50% of the spherical particles have particle size diameter averaged 9.50 nm. The observed small aggregates could be attributed to evaporation of the solvent throughout the TEM examination, in Fig. 3**.** The XRPD pattern has shown typical noisy and broad peak centered around 24.50° that corresponds to 0.34 nm interlayer spacing and could be attributed to the high distortion of carbon atoms by doping with heteroatoms. This assigns clearly the graphite structure and hence confirms the formation of QDs (Zhu et al. 2013), in Fig. 4.

The quantum yield (QY) measurements

The determination of the QY of the synthesized PNQDs was achieved as a comparative study. A solution of quinine sulfate in 0.10 M H_2SO_4 was utilized as reference. The UV absorbances of the quinine sulfate solution and the colloidal aqueous solution of the PNQDs were measured at 350 nm and kept below 0.10. The QY was calculated according to Eq. (1), **(**Liang et al. 2013):

$$\phi_c = \phi_q \left(\frac{A_c}{A_q}\right)\left(\frac{I_c}{I_q}\right)\left(\frac{\eta_c}{\eta_q}\right) \quad (1)$$

where the subscripts "*q*" and "*c*" refer to the quinine sulfate solution and the PNQDs colloidal aqueous solution, respectively, ϕ is the QY (ϕ_q is 54.00%), A is the absorbance at the excitation wavelength, 350 nm, and η is the refractive index of the solvent.

The calculated QY (ϕ_c) was found to be 3.50%. In spite of the low value of the QY value, successful monitoring of the RIB concentration and its ssDNA binding interaction has taken place. Furthermore, the obtained QY is quite similar to the previously synthesized QDs of natural sources and used efficiently in detection and bioimaging through an eco-friendly concept (Wang et al. 2014; Nair et al. 2020).

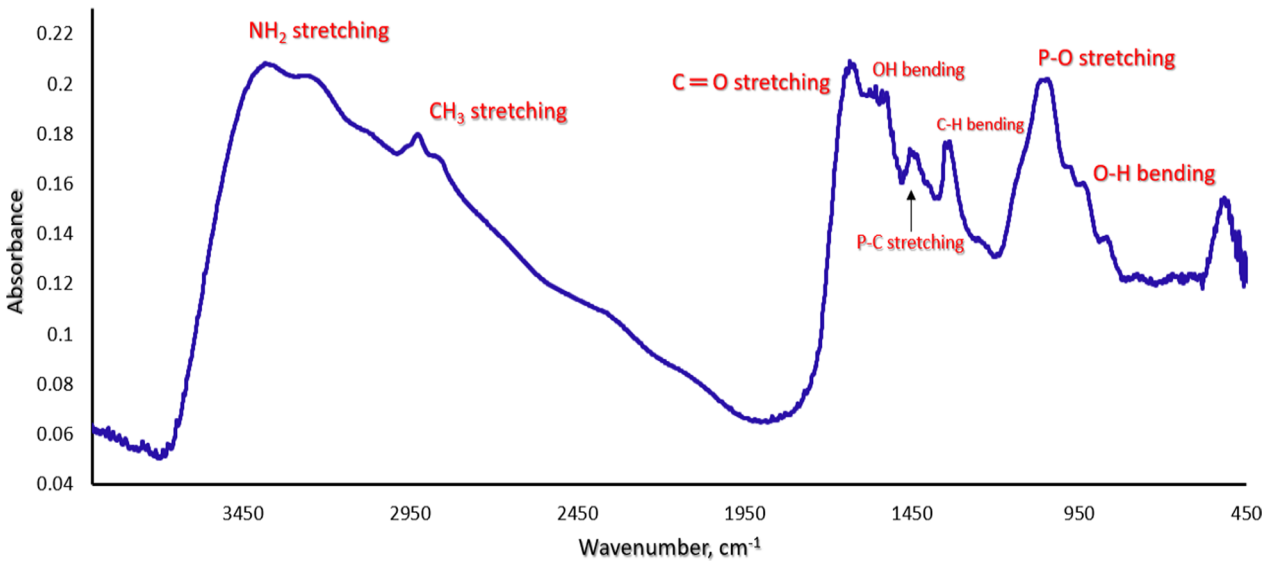

Fig. 2 The FTIR spectrum of the synthesized PNQDs

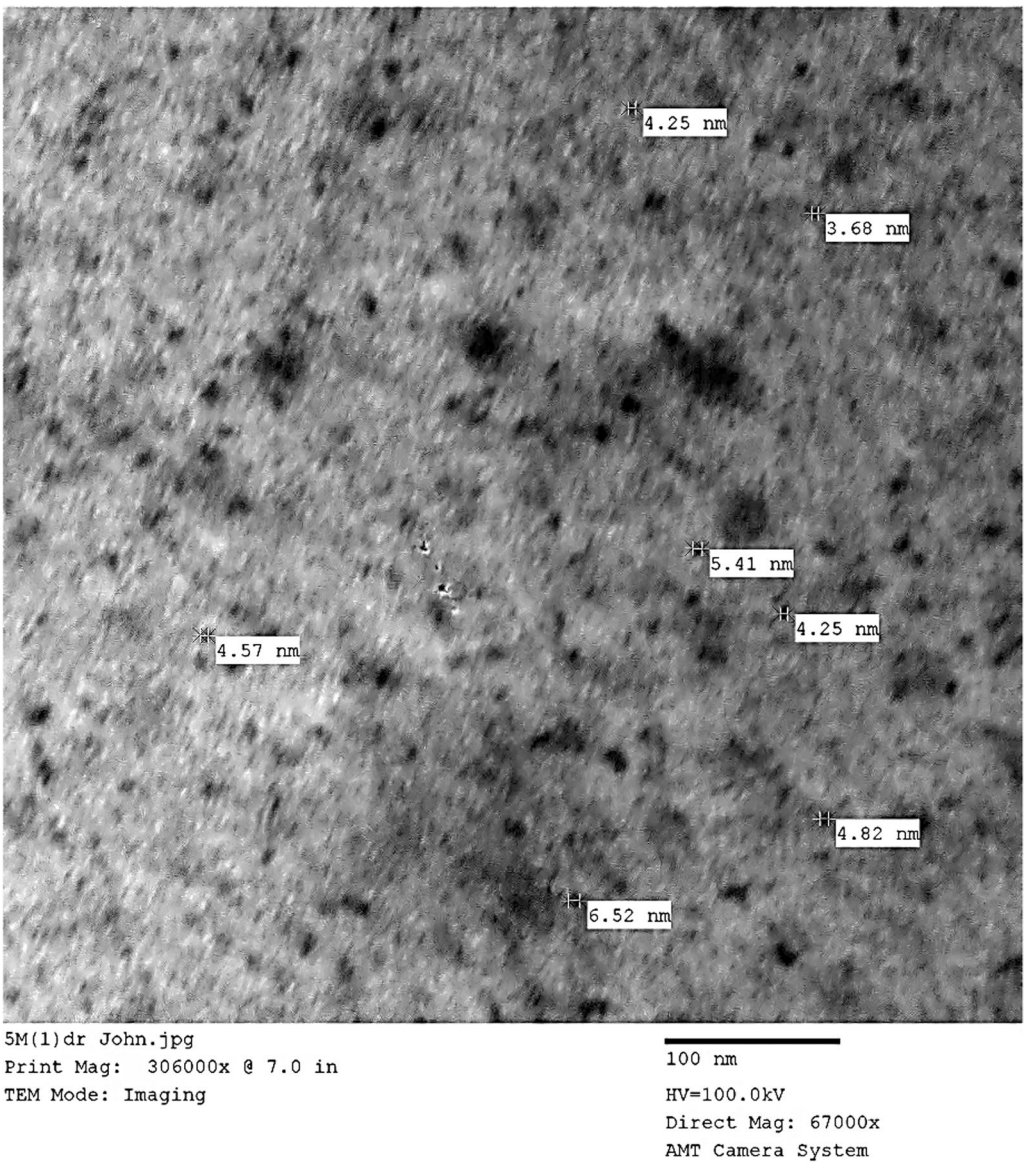

Fig. 3 The typical TEM image of the synthesized PNQDs

Preparation of buffer solutions

Potassium dihydrogen phosphate solution of 5.00×10^{-3} M concentration was utilized for preparation of phosphate buffer solutions by adjustment of 90.00 mL volumes with either H_3PO_4 or 1.00×10^{-2} M NaOH to get pH range of 2.00–8.00 (USP30-NF25. United State Pharmacopoeia 30-National Formulary 25 2007). Borate buffer (pH 10.00) was prepared by dissolving 2.46 g boric acid in 90.00 mL double-distilled water. The pH value was then adjusted to pH 10.00 by the NaOH solution, and afterward, it was completed to 100.00 mL by the same solvent (British Pharmacopoeia, vol. III. London: Her Majesty's Stationery 2007).

Preparation of the PNQDs colloidal solution

The stock solution of 1.00 mg/mL was prepared by dispersing 100.00 mg PNQDs in distilled water to get 100 mL colloidal solution. Further dilutions were made by phosphate buffer (pH 4.00) for RIB determination studies and by tris–HCl for the ssDNA binding assessment studies.

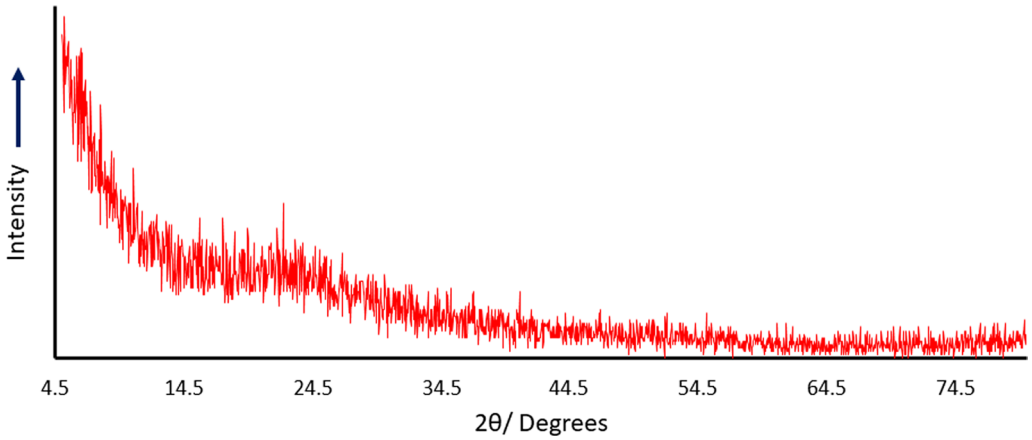

Fig. 4 The XRPD pattern of the synthesized PNQDs

Preparation of the ssDNA solution

Into a 100.00-mL volumetric flask, 20.00 mg ssDNA was dissolved in 5.00×10^{-3} M Tris–HCl aqueous solution and then made up to the mark by the same solution. The obtained solution was covered with aluminum foil and kept away from light in the refrigerator at 4 °C for one week (Abdel Hakiem et al. 2023). Afterwards, the concentration was measured at 260 nm for a molar absorptivity (ε) of 6600 L mol^{-1} cm^{-1} (Bi et al. 2012) and path length (b) of 1.00 cm to be 310.20 µM. Further dilutions have been made with Tris–HCl solution to get working solutions concentration range of 5.00–50.00 µM. The purity of the ssDNA has been assessed in accordance with our previous report (Abdel Hakiem et al. 2023). The absorbance ratio at 260/280 nm was checked to be $>$ 1.80 indicating protein-free composition.

Preparation of RIB standard solutions

The stock standard solutions of 1.00 mg/mL were prepared by dissolving 100.00 mg pure RIB in phosphate buffer solution (pH 4.00) and Tris–HCl solution (pH 7.40). These solutions were then made up to 100.00 mL by the same solutions. Afterwards, further dilutions have been made by the same solutions to obtain the required working concentrations.

Preparations for the zeta potential study

In respect, RIB determination study, zeta potential was measured for a prepared number of (1:1, v/v) mixtures, containing fixed concentration of PNQDs (6.00 µg/mL) and different concentrations of RIB (1.50–10.00 µM). On the other hand, to investigate the RIB–ssDNA interaction, a complex is first prepared between the RIB (6.00 µM) and the PNQDs (6.00 µg/mL) in ratio (1:1, v/v). Zeta potential was then assessed for different concentrations of ssDNA (0.60–3.00 µM) mixed with the previously prepared mixture in ratio (1:1, v/v). Both studies have taken place in reaction times of three minutes.

Application to the pharmaceutical formulations

The contents of ten Ribavirin® capsules (200.00 mg, MinaPharm for Pharmaceutical Industry, Egypt) were accurately weighed. An amount equivalent to 10.00 mg RIB was transferred into 10.00 mL volumetric flask and diluted by 5.00 mL phosphate buffer solution (pH 4.00), then sonicated for thirty minutes. Afterwards, it was made up to the mark by the same solution and shaken well. The obtained solution was filtered and the supernatant was subjected to further dilutions to obtain a working solution of 30.00 µg/mL.

Application to the spiked human plasma samples

Into 15-mL falcon tubes, one milliliter of drug-free human plasma was spiked with one milliliter of RIB working solutions in the concentration ranges of (6.00–1000.00 µg/mL). Two milliliters of acetonitrile was added to each tube to denature the protein content then the tubes were vortexed for 1 min. Finally, the tubes were completed with phosphate buffer solution (pH 4.00) to 10.00 mL and centrifuged for 25 min at 10,000 rpm. One milliliter volumes of the clear supernatants of each tube were transferred into 10-mL volumetric flasks and completed to the mark with phosphate buffer solution (pH 4.00) to obtain final RIB concentration range of (0.06–10.00 µg/mL).

The general analytical procedures

Into a series of 10-mL volumetric flasks, serial dilutions of the stock standard solution have been prepared using phosphate buffer solution pH 4.00 to get the concentration range of 0.06–10.00 µg/mL. The RIB (different concentrations)–PNQDs (6.00 µg/mL) mixtures have been prepared in ratio (1:1, v/v). After reaction time of three minutes, the fluorescence intensities of RIB–PNQDs mixtures have been measured at 401 nm following excitation at 245 nm The calibration curves were constructed by plotting F_o/F versus the concentration of RIB in µg/mL.

Results and discussion

Optimization study

Fluorescence intensity of the PNQDs

Different concentrations (0.0125–7.00 µg/mL) of the PNQDs colloidal aqueous solutions have been investigated for the fluorescence intensity at $\lambda_{excitation}$ and $\lambda_{emission}$ of 245 and 401 nm, respectively. The effect of the potentially affecting parameters on the fluorescence intensity has been studied like the pH value (adjusted by phosphate and borate buffers in the pH range 2.00–10.00) and the ionic strength of NaCl (0.10–1.00 M).

A gradual increase in the fluorescence intensity has been observed by increasing the PNQDs concentration, and then, a plateau has begun from almost 4.50 µg/mL; hence, 6.00 µg/mL was selected as mid-plateau point, in Fig. 5. This plateau could be attributed to that all incident radiation will be absorbed and fluorescence will be independent on the concentration of the PNQDs owing to Eq. (2).

$$F = I^0\phi \tag{2}$$

where F is the fluorescence intensity, I^0 is the incident light, and ϕ is the quantum yield

A great decline in fluorescence intensity from pH 2.00 to pH 3.00 was observed. It is reasonable to believe that at this pH range, the surface charge disturbances like protonation and development of quaternary nitrogen have taken place; consequently, repulsive forces have improved and hence, losing energy in non-radiational forms (i.e., internal conversion and vibrational relaxation). Hence, it hinders the fluorescence intensity significantly. A plateau region from pH 3.00 to pH 6.00 has been observed, at which pH 4.00 was selected for RIB determination studies as a mid-point within the plateau. A slight further decline from pH 6.00 to pH 10.00 has taken place and this could be attributed to development of negatively charged carboxylate moieties that impart further repulsion to the PNQDs and consequently more inner filter effects, in Fig. 6

Based on the fact that, ionic interference caused by the ionic strength of salts could determine whether the QDs become much closer or away from each other by modification of surface charges together with pH effect (Qiang et al. 2019). It has been evidenced in this study that fluorescence intensity has not been affected by the electrolyte concentration all over the studied NaCl concentration range (0.10–1.00 M), in Additional file 1: Figure (S1).

Interaction assessment between the PNQDs, RIB and ssDNA

The optimization of the factors affecting the interaction between RIB and the PNQDs A number of experimental parameters that are highly affecting the binding interac-

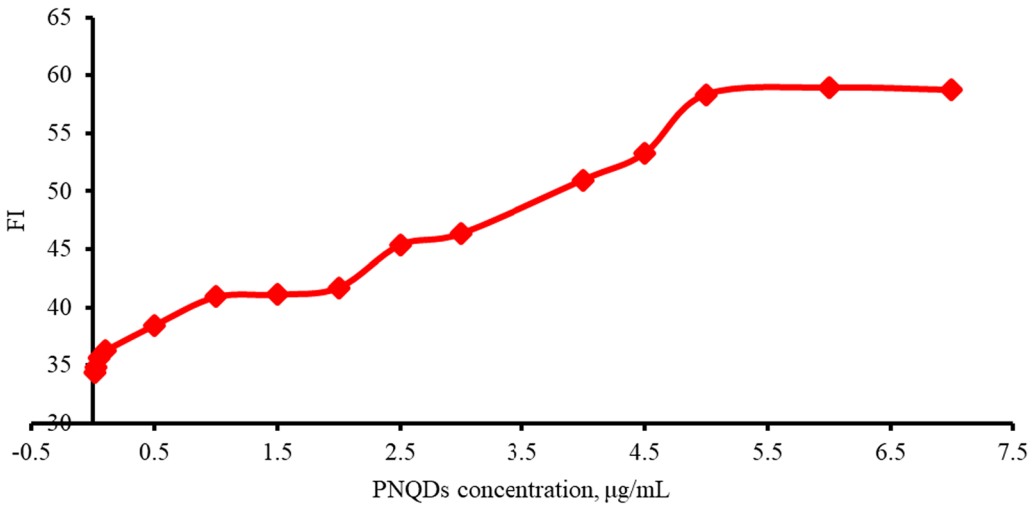

Fig. 5 The concentration of PNQDs and fluorescence intensity

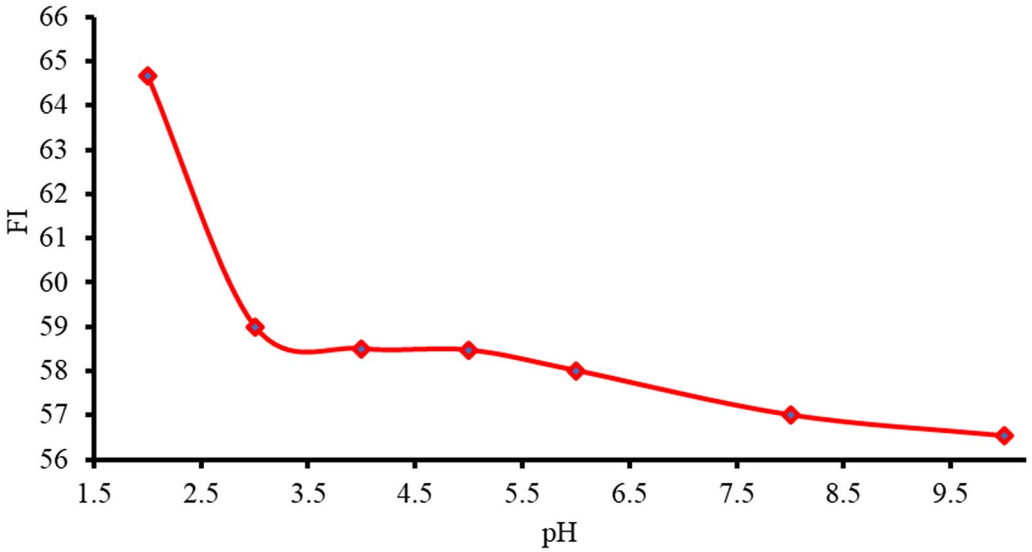

Fig. 6 The effect of pH on PNQDs (6.00 µg/mL) fluorescence intensity

tion between RIB (6.00 µg/mL) and the PNQDs (6.00 µg/mL) have been investigated, namely the pH value (2.00–12.00), the buffer concentration (0.01–0.07 M) and the reaction time (1–10 min).

Ribavirin is a basic drug having pKa value of 12.95. The amide moiety and the triazole ring are considered the characteristic structural features. At the strongly acidic medium from pH 3.00 to pH 3.50, protonation has taken place in both the PNQDs and the RIB molecules. In concern the PNQDs, the surface amino groups have been protonated and become positively charged quaternary amino moeities. On the other hand, the amino groups of the amide moiety in RIB molecule have been also protonated as well as the triazole ring which has been stabilized by resonance. Accordingly, strong repulsive forces have arisen between the RIB molecules and the PNQDs that favor also the PNQDs to remain in their colloidal state and hence minimize the possibility of self-quenching or inner filter effect. This interprets the increase in fluorescence intensity at this pH range. No more significant protonation could happen up to pH 8.00; hence, the fluorescence intensity remained almost constant giving a

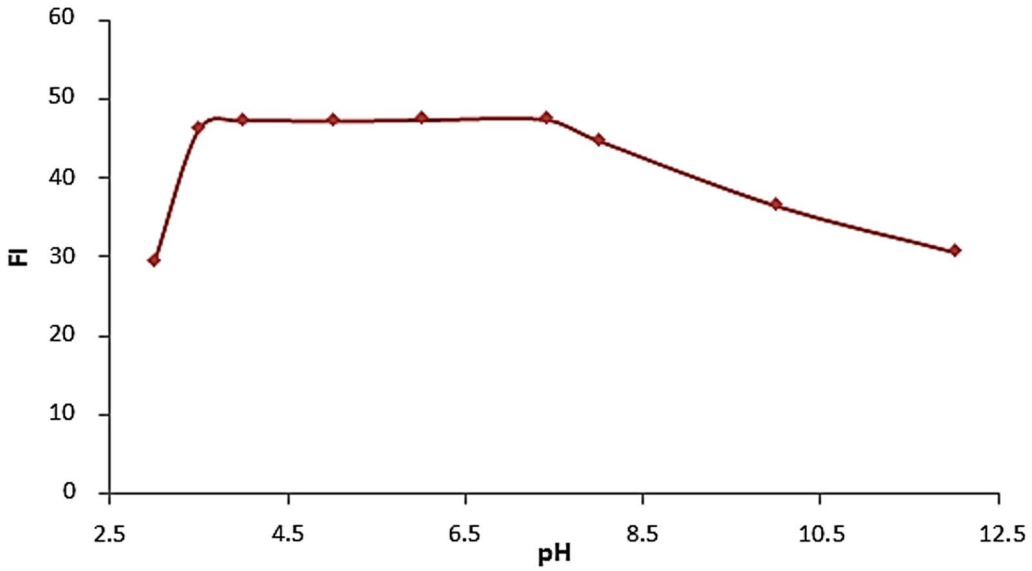

Fig. 7 The effect of pH on PNQDs (6.00 µg/mL)–RIB (6.00 µg/mL) interaction

plateau region. At the highly basic conditions (pH 8.50–12.50) deprotonation of the amino moieties and the triazole ring giving a possibility aggregation and conjugation between the RIB molecules and the PNQDs commonly by non-electrostatic forces. Consequently, decay in fluorescence in this pH range has taken place. The pH value of 4.00 within the plateau region was chosen for the RIB determinations. On the other hand, only the pH value of 7.40 (the physiological pH) is chosen for the interaction study between the RIB molecules and the ssDNA because of the necessity for the ssDNA stability at this physiological pH (Uhlenhopp and Krasna 1969), in Fig. 7.

The assembly between the RIB molecules and the PNQDs was tested under increasing buffer concentration (0.01–0.07 M) because of its disruptive effect to the electrostatic interactions (Dennis et al. 2010). As shown in Additional file 1: Figure S2, the ionic strength is found to have no significant effect on interaction between the PNQDs and RIB.

The effect of the reaction time was investigated from 1 min up to 10 min. Almost significant reduction in fluorescence intensity took place in the first minute followed by stable fluorescence intensity. This indicates the completion of the interaction at the second minute, and hence, a reaction time of three minutes was considered throughout the study, in Additional file 1: Figure S3.

The mechanism of the fluorescence sensing by RIB molecules

The quenching mode Ribavirin has exhibited significant quenching effect on the native fluorescence of PNQDs, in Fig. 8. The fluorescence quenching could be dynamic as a result of collisions between the quencher and the fluorophore or static which is attributed to formation of a ground state complex between them (Lakowicz 2006; Wang et al. 2019).

The fluorescence response of the PNQDs versus the added concentration of the quencher (RIB) was represented in the light of the Stern–Volmer equation, **Eq.** (3) (Peng et al. 2019; Liu et al. 2020);

$$F_0/F = K_{sv}[\text{Quencher}] + 1 = K_q\tau_0[\text{Quencher}] + 1 \quad (3)$$

where F_0 is the fluorescence intensity of PNQDs before addition of RIB, F is the fluorescence intensity of PNQDs after addition of RIB, K_{sv} is the Stern–Volmer constant, K_q is the bimolecular quenching rate constant, [Q] is the concentration of the quencher, and τ_0 is the average lifetime of the fluorophore in the excited state and its value is usually 10^{-8} s for biomolecules. The mode of quenching or complex formation (i.e., static quenching) is obtained from the value of K_q which equals K_{sv}/τ_0. Good linear fittings were obtained by construction of F_o/F versus the concentration of RIB in authentic and spiked

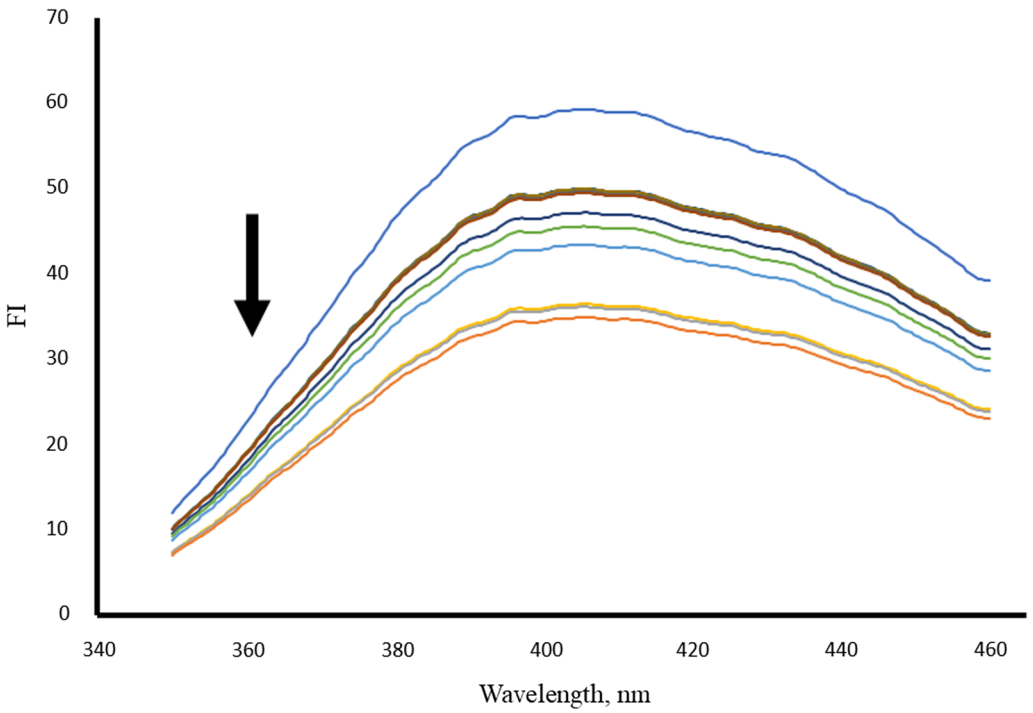

Fig. 8 Quenching effect of RIB in the concentration range (0.06–10.00 µg/mL) to the native fluorescence of the synthesized PNQDs (6.00 µg/mL)

human plasma samples for good correlation coefficients of 0.9998 and 0.9830, respectively. For the dynamic quenching, the value of the maximum scattering collision constant of different quenchers is 2.00×10^{10} L M^{-1} S^{-1}. Consequently, the much higher K_q values derived from the linear regression equations: 1.30×10^{12} L M^{-1} S^{-1} and 1.73×10^{12} L M^{-1} S^{-1}, in authentic and in spiked plasma samples have evidenced the static quenching mechanism. Additionally, although the Stern–Volmer equation suits both static and dynamic quenching modes, the dependence of the slope (K_{sv}) on the quencher concentration has furtherly confirmed the static quenching rather than that of the dynamic one which is not responsive to concentration changes (Xiang et al. 2007; Qi et al. 2008).

Zeta potential measurements The value of the resultant zeta potential is highly considered for assessment of the ligand–QDs interaction. It is considered a representing term for the actual surface charge affecting the electrokinetic potential arising at the interfacial double layer between the QDs surface and solution of the ligand (Honary and Zahir 2013). The more the dispersion surface charge (zeta potential) either positive or negative, the greater the surface charge, resulting in development of repulsive forces causing deagglomeration of particles. It is considered an indicator for the colloidal stability, i.e., the more the zeta potential, the higher the colloidal stability. While the surface charge reduction on the PNQDs is attributed to strong binding of the ligand, hence, the smaller the potential, the more the attractive forces and flocculation exceeding repulsion and dispersion forces (Kanagasubbulakshmi and Kadirvelu 2018). Its value is mainly dependent on the concentration, ionic strength and the pH value (Leong et al. 2020).

The binding interaction between RIB and PNQDs was clearly exhibited from zeta potential measurements that have shown continuous decrease in the numerical value of the negative potential by increasing the added

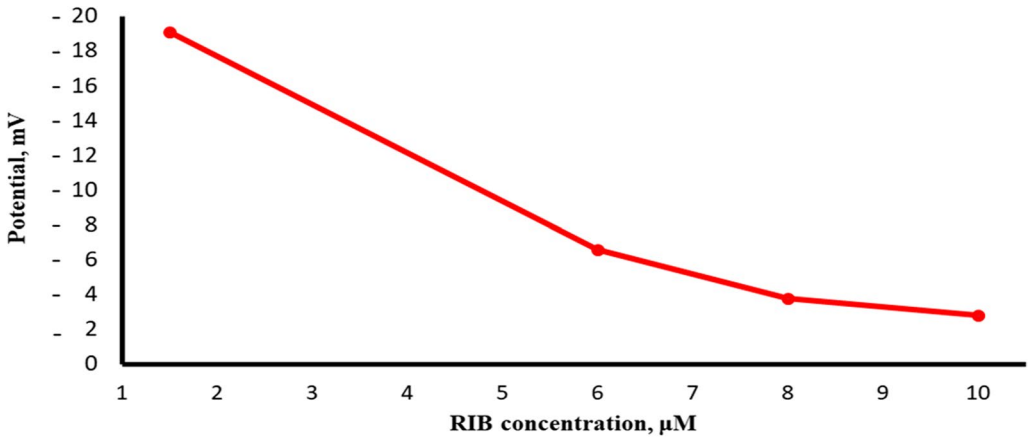

Fig. 9 Zeta potential of a PNQDs fixed concentration (6.00 µg/mL) at increased added RIB concentration

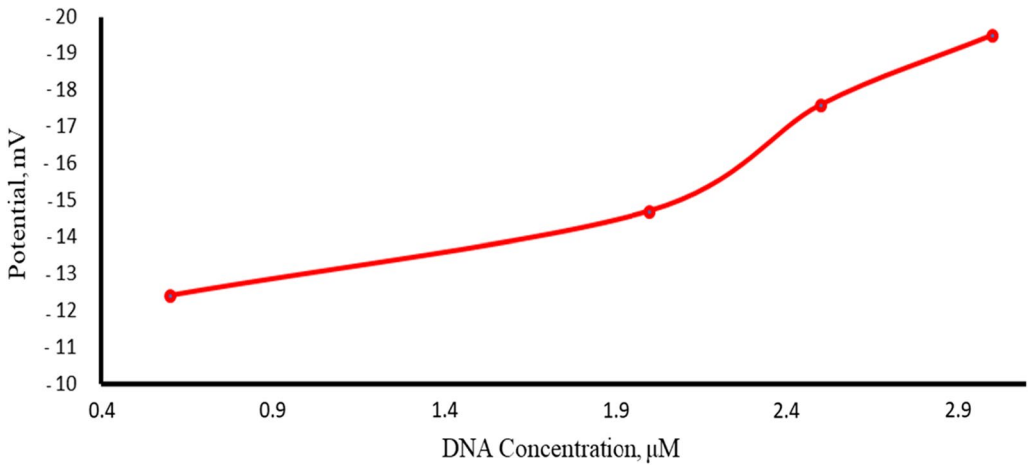

Fig. 10 Zeta potential of the fixed concentration of PNQDs (6.00 µg/mL)–RIB (6.00 µg/mL) complex at increased added ssDNA concentration

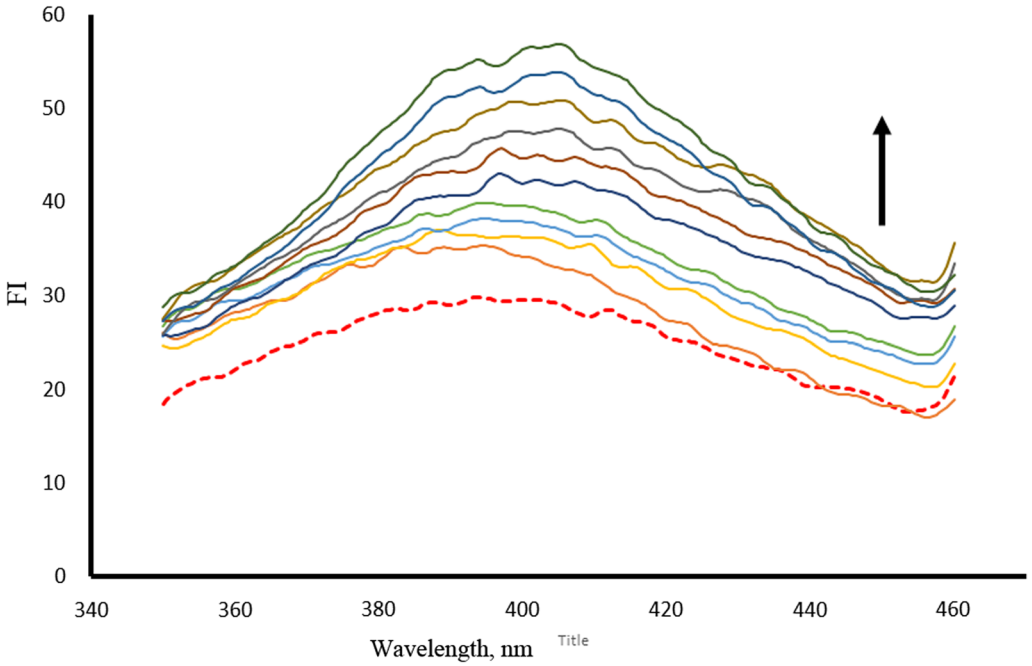

Fig. 11 Turning on of the PNQDs (6.00 µg/mL)–RIB (6.00 µg/mL) upon titration with ssDNA in the concentration range (5.00–50.00 µM)

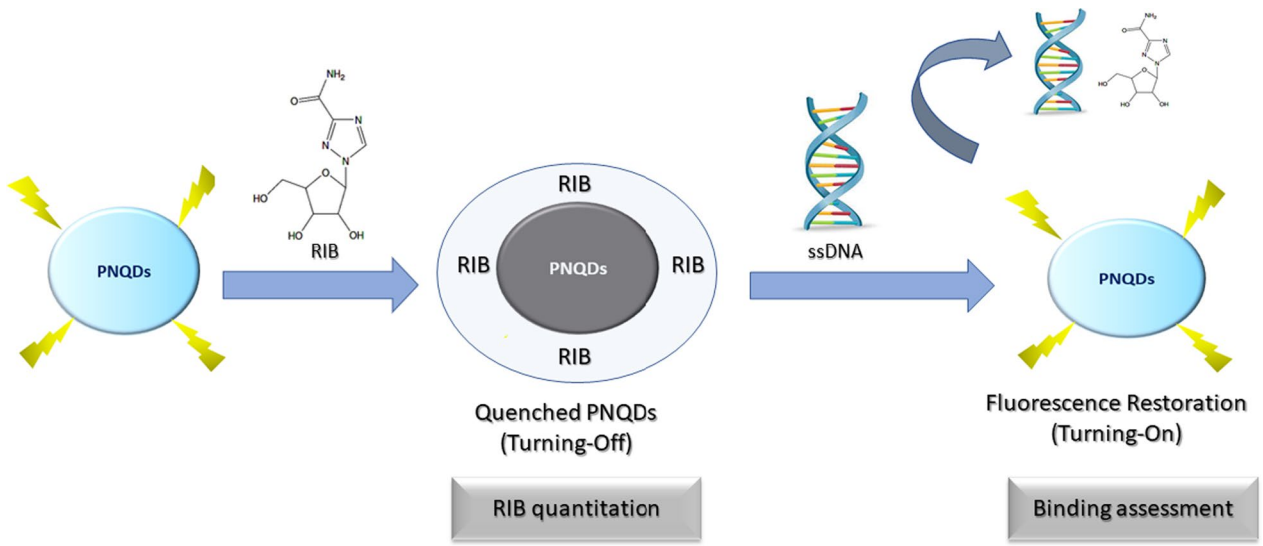

Scheme 2 Turning-off-on switching of the PNQDs for assessment of RIB concentration and its binding interaction to ssDNA.

concentrations of RIB. This indicates enhanced tendency for assembly and aggregation and hence fluorescence quenching or turning off, in Fig. 9. On the other hand, upon successive addition of the ssDNA to the PNQDs–RIB complex, an increase in zeta potential (turning on) was obtained illustrating the ability of RIB to interact with ssDNA and detach it from the surface of PNQDs, and hence the fluorescence restoration (turning on) in Fig. 10.

The binding interaction study between RIB and ssDNA The ssDNA possesses very weak fluorescence, hence by addition of increased concentration of ssDNA solution to the PNQDs–RIB complex, a gradual restoration (turning on) of the PNQDs fluorescence has been obtained, in Fig. 11, Scheme 2. This was evidenced furtherly by the increasing zeta potential upon successive addition of the ssDNA, in Fig. 10. Consequently, the PNQDs are considered as fluo-

rescent probes for indirect determination of the binding interaction between the RIB molecules and the ssDNA.

Traditionally, the fluorescence restoration rate of PNQDs could explain the ability of RIB to interact with ssDNA. This assessment overrides the quenched fluorescence intensity variation ascribed to the added different concentrations of the quencher (RIB). By plotting the fluorescence enhancement factor, $(F–F_0)/F_0$ as percentage versus concentration of the added ssDNA (Liu et al. 2017), an excellent correlation ($R^2=0.9992$) was obtained confirming the peeling off ability of the ssDNA to the RIB molecules, in Additional file 1: Figure S4, where F_0 is the original fluorescence intensity, and F is the restored fluorescence intensity. The binding constant between RIB and the ssDNA was successfully estimated utilizing the spectral characters of the PNQDs as fluorescent probes by competing and peeling off the electrostatically surface absorbed RIB molecules using **Eq.** (4) (Hu et al. 2014):

$$\frac{C}{I}=\frac{1}{K_b I_{max}}+\frac{1}{I_{max}}C \quad (4)$$

where C is the concentration of ssDNA, I is the fluorescence intensity of the PNQDs at a given ssDNA concentration, I_{max} is the maximum fluorescence intensity of the PNQDs restored by the presence of ssDNA, and K_b is the binding constant. By construction a plot between C/I versus the added concentration of the ssDNA in the molar concentration, a good linear regression relationship ($y=0.0158x+2\times10^{-7}$) for R^2 value of 0.9621 has been obtained. A binding constant (K_b) of 7.9×10^4 mol^{-1}/L was derived of the previous relationship depicting high conjugation between RIB and the ssDNA. Hence, RIB could be considered as potent molecule against the DNA viruses as well as the malignant cells for future clinical studies, in Additional file 1: Figure S5.

The validation study

The proposed method was validated according to the ICH guidelines (Ich 2005). The linearity and range were investigated in authentic and spiked human plasma samples by plotting the RIB concentration against the relative fluorescence intensity; F_0/F, while F_0 and F are the fluorescence intensities in the absence and the presence of RIB, respectively. The accuracy was investigated as percentage recoveries at three concentration levels: low, mid and high of the obtained linear range. The precision was studied as percentage relative standard deviation (% RSD) at three concentration levels covering the linearity range within the day (intra-day) and in subsequent working days (inter-day). The robustness was determined by inspecting the effect of faint variation in the optimization parameters: reaction time, pH of the reaction medium and the concentration of the QDs.

Linearity and range

Good linearity ranges were obtained for both authentic and spiked plasma samples in the range from 0.06 up to 10.00 µg/mL. The authentic and spiked plasma samples have exhibited excellent correlation coefficients (r) of 0.9998 and 0.9830, respectively, in Table 1.

Table 2 Accuracy study of ribavirin by the proposed method

	Taken (µg/mL)	Found[a] (µg/mL)	% Recovery
Low	0.12	0.12	99.45
Mid	4.00	3.91	97.65
High	10.00	9.88	98.86
Mean			98.65
SD			0.91
%RSD			0.93

SD standard deviation, *RSD* relative standard deviation

[a] Average of three determinations

Table 1 Linearity parameters of RIB by the proposed method as authentic and in spiked human plasma samples

Parameters	Authentic samples	Spiked plasma
Linearity range (µg/mL)	0.06–10.00 ≈ 2.46×10^{-7} M–4.09×10^{-5} M	0.06–10.00 ≈ 2.46×10^{-7} M–4.09×10^{-5} M
Correlation coefficient (r)	0.9998	0.9830
Determination coefficient (R^2)	0.9997	0.9663
Slope (b)	0.0527	0.0577
SD of slope	0.00556	0.00353
Intercept (a)	1.18	1.17
SD of intercept	0.00023	0.000295
LOD (µg/mL)	0.014	0.016
LOQ (µg/mL)	0.04	0.05

Table 3 Precision study for the developed method

Parameters	0.12 µg/mL	4.00 µg/mL	10.00 µg/mL
Intra-day*	99.45	97.65	98.86
	98.36	97.34	99.23
	97.28	99.12	99.70
Mean	98.36	98.04	99.27
SD	1.08	0.94	0.42
%RSD	1.10	0.96	0.42
Inter-day*	99.45	97.65	98.86
	101.62	100.50	97.94
	100.17	99.27	98.77
Mean	100.42	99.14	98.52
SD	1.10	1.43	0.51
%RSD	1.10	1.44	0.51

*Average of three determinations

Table 4 Robustness results for the developed method

Parameters	The small variations[a]	% RSD
Reaction time (3 min ± 30 sec)	2.5 min	0.93
	3 min	0.84
	3.5 min	0.88
pH (4.00 ± 0.20)	3.80	1.06
	4.00	1.03
	4.20	0.97
Concentration of quantum dot (6.00 ± 0.20 µg/mL)	5.80 µg/mL	0.99
	6.00 µg/mL	0.94
	6.20 µg/mL	0.91

[a] Average of three determinations

Limits of detection and quantitation

Sensitivity of the proposed method was assessed through obtaining limits of detection (LOD) and quantitation (LOQ), in Eqs. (5 and 6).

$$\mathrm{LOD} = \left(3.3^{*}\,\sigma\right)/S \tag{5}$$

$$\mathrm{LOQ} = \left(10^{*}\,\sigma\right)/S \tag{6}$$

Table 6 Application of the proposed method to spiked human plasma samples

Taken (µg/mL)	Found[a] (µg/mL)	% Recovery
2.00	2.06	103.47
4.00	4.13	103.44
6.00	6.26	104.35
8.00	8.28	103.50
10.00	10.33	103.30
Mean		103.61
SD		0.41
%RSD		0.40

[a] Average of three determinations

where (σ) is the standard deviation of intercept and (S) is the average slope. The limits of detection and quantitation were calculated to be 0.014 and 0.04 µg/mL for authentic material and 0.016 and 0.05 µg/mL for spiked human plasma. This indicates the excellent sensitivity of the proposed method, in Table 1.

Accuracy, precision and robustness studies

The monitored three concentrations for the accuracy study at low and mid and high levels of the linearity range have shown excellent recovery percentages ranged from 97.65 to 99.45%, in Table 2. Both the intra-day (repeatability) and inter-day precision investigations have shown % RSD values of not more than 1.50 indicating the reliability of the proposed method, in Table 3. The robustness study has proven that minor changes of the investigated optimization parameters (i.e., reaction time, pH value and the concentration QDs) had not affected significantly the determination of RIB with % RSD values not exceeding 1.10, in Table 4.

Application to pharmaceutical formulations and spiked plasma samples

Ribavirin has shown good recovery of 102.81% upon application of the proposed method to the commercially available Ribavirin.® capsules. The proposed

Table 5 Determination of RIB in its pharmaceutical formulations by the proposed method and statistical comparison with a reported HPLC method

Pharmaceutical formulation	Equivalent concentration of analytes (µg/mL)	% Recovery[a] by the developed method ± SD	Claimed amount (mg)	% Recovery[a] by the reported methods ± SD	*t*-test[b]	F-test[b]
Ribavirin® capsules (200.00 mg)	4.00	102.81 ± 0.64	205.62	103.69 ± 1.09	1.70	2.87

[a] The values are the mean of five determinations

[b] The tabulated values of *t*-test and F test at 0.05% are 2.306 and 5.05, respectively

method has been compared with a previously reported HPLC–DAD detection method (Haggag et al. 2014). The comparison has taken place using Student's *t* test and F test at 95% confidence level. The results have proven no significant differences demonstrating no excipient interferences, in Table 5. It was evidenced that the plasma components are slightly interfering with the RIB determination. The obtained percentage recoveries are averaged 103.60% for the investigated concentration range: 2.00–10.00 µg/mL. It was reported that the maximum plasma concentration (C_{max}) of RIB is 4.18 ± 0.20 µg/mL (Martin and Jensen 2008), and hence, this depicts the suitability of the proposed method for in the vivo analysis, in Table 6

Conclusion

A spectrofluorimetric "turn off–on" approach has been utilized for sensitive determination of the antiviral agent, RIB as well as assessment of its interaction with the ssDNA. For this purpose, eco-friendly fluorescent nanosensors have been synthesized from pure orange juice, ethylenediamine and phosphoric acid. These nanoparticles have acted as sensitive fluorescent platforms that have been quenched by the non-fluorescent RIB molecules (turning off) and the quenching was proven to be static. Wide linearity ranges have been obtained in authentic and spiked plasma samples with LOQ values down to 60.00 ng/mL. The proposed method has been validated efficiently in accordance with the ICH guidelines. Excellent recoveries were obtained upon application to the commercial tablets and spiked plasma samples. It was evidenced that there is no significant difference by comparison with a previously reported method. Upon titration of RIB–PNQDs complex with ssDNA, fluorescence restoration has taken place. This was exploited to calculate the high binding constant of RIB to ssDNA revealing its excellent antiviral activity. Consequently, this could be considered new era in repurposing as anticancer or enhancement of RIB therapeutic spectrum.

Supplementary Information

The online version contains supplementary material available at https://doi.org/10.1186/s40543-023-00391-4.

Additional file 1. Supplementary file.

Acknowledgements

The authors would like to express their gratitude to GLOBAL NAPI Pharmaceuticals (Giza, Egypt) for providing the supplies needed to complete this study.

Funding

Open access funding provided by The Science, Technology & Innovation Funding Authority (STDF) in cooperation with The Egyptian Knowledge Bank (EKB). This research did not receive any specific grant from funding agencies in the public, commercial, or not-for-profit sectors.

Availability of data and materials

All data generated or analyzed during this study are included in this published article [and its supplementary information files].

Declarations

Competing interests

The authors declare that they have no known competing financial interests or personal relationships that could have appeared to influence the work reported in the manuscript.

Author details

[1]Pharmaceutical Analytical Chemistry Department, Faculty of Pharmacy, South Valley University, Qena 83523, Egypt. [2]Pharmaceutical Chemistry Department, Faculty of Pharmacy, Nahda University, Beni-Suef 62521, Egypt. [3]Analytical Chemistry Department, Faculty of Pharmacy, Minia University, Minia 61519, Egypt.

Received: 23 February 2023 Accepted: 11 June 2023
Published online: 29 June 2023

References

Abdel Hakiem AF, El-Sagheir AMK, Draz ME, Mohamed NA, Aboraia AS. Assessment of binding interaction to salmon sperm DNA of two antiviral agents and ecofriendly nanoparticles: comprehensive spectroscopic study. BMC Chem. 2023;17(1):1–13. https://doi.org/10.1186/s13065-023-00952-z.

Alhazzani K, Alanazi A, Alaseem AM, Al Awadh SA, Alanazi SA, AlSayyari AA, et al. A reliable ratiometric fluorescence sensing of heparin and its antidote based on cationic carbon quantum dots and acid red 87. Microchem J. 2023;190:108666. https://doi.org/10.1016/j.microc.2023.108666.

Ali MJ, Hanif M, Haider MA, Ahmed MU, Sundas F, Hirani A, et al. Treatment options for COVID-19: a review. Front Med. 2020;7:480. https://doi.org/10.3389/fmed.2020.00480.

Ali HR, Mohamed NA, Hakiem AFA. Facile determination of ezetemibe and either atorvastatin or simvastatin by Fourier transform infrared spectroscopy. Vib Spectrosc. 2021;115:103273. https://doi.org/10.1016/j.vibspec.2021.103273.

Alqahtani YS, Mahmoud AM, El-Wekil MM. Bifunctional nanoprobe for dual-mode detection based on blue emissive iron and nitrogen co-doped carbon dots as a peroxidase-mimic platform. Talanta. 2023;253:124024. https://doi.org/10.1016/j.talanta.2022.124024.

Badıllı U, Mollarasouli F, Bakirhan NK, Ozkan Y, Ozkan SA. Role of quantum dots in pharmaceutical and biomedical analysis, and its application in drug delivery. TrAC Trends Anal Chem. 2020;131:116013. https://doi.org/10.1016/j.trac.2020.116013.

Benítez-Martínez S, Valcárcel M. Fluorescent determination of graphene quantum dots in water samples. Anal Chim Acta. 2015;896:78–84. https://doi.org/10.1016/j.aca.2015.09.019.

Bi S, Yan L, Wang Y, Pang B, Wang T. Spectroscopic study on the interaction of eugenol with salmon sperm DNA in vitro. J Lumin. 2012;132(9):2355–60. https://doi.org/10.1016/j.jlumin.2012.04.029.

Breadmore MC, Theurillat R, Thormann W. Determination of ribavirin in human serum and plasma by capillary electrophoresis. Electrophoresis. 2004;25(10–11):1615–22. https://doi.org/10.1002/elps.200305819.

Dennis AM, Sotto DC, Mei BC, Medintz IL, Mattoussi H, Bao G. Surface ligand effects on metal-affinity coordination to quantum dots: implications for nanoprobe self-assembly. Bioconjug Chem. 2010;21(7):1160–70. https://doi.org/10.1021/bc900500m.

El-Shaboury SR, El-Gizawy SM, Atia NN, Abo-Zeid MN. Validated spectrodensitometric method for simultaneous estimation of sofosbuvir, ribavirin and

saxagliptin in their pure and pharmaceutical dosage forms. Curr Pharm Anal. 2018;14(3):212–8. https://doi.org/10.2174/1573412913666170210151615.
El-Yazbi AF, Khalifa Y, Elkhatib MA, El-Yazbi AF. Green analytical method for the determination of sofosbuvir, ledipasvir, ribavirin and complex silymarin flavonoids simultaneously in biological fluids. Microchem J. 2021;164:105964. https://doi.org/10.1016/j.microc.2021.105964.
Franca AS, Nollet LM. Spectroscopic methods in food analysis. Boca Raton: CRC Press; 2017.
Haggag RS, Belal SF, Hewala II, El Rouby OA. Stability-indicating HPLC–DAD determination of ribavirin in capsules and plasma. J Chromatogr Sci. 2014;52(6):493–500. https://doi.org/10.1093/chromsci/bmt067.
Hakiem AFA, Kendrick J, Ali HRH. Towards understanding of different solid forms of formoterol fumarate: combined computational and experimental approach. Vib Spectrosc. 2020;110:103132. https://doi.org/10.1016/j.vibspec.2020.103132.
Hakiem AFA, Mohamed NA, Ali HR. FTIR spectroscopic study of two isostructural statins: simvastatin and Lovastatin as authentic and in pharmaceuticals. Spectrochim Acta Part A Mol Biomol Spectrosc. 2021;261:120045. https://doi.org/10.1016/j.saa.2021.120045.
Homma M, Jayewardene AL, Gambertoglio J, Aweeka F. High-performance liquid chromatographic determination of ribavirin in whole blood to assess disposition in erythrocytes. Antimicrob Agents Chemother. 1999;43(11):2716–9. https://doi.org/10.1128/AAC.43.11.2716.
Honary S, Zahir F. Effect of zeta potential on the properties of nano-drug delivery systems-a review (Part 1). Trop J Pharm Res. 2013;12(2):255–64. https://doi.org/10.4314/tjpr.v12i2.19.
Hu X, Zhu K, Guo Q, Liu Y, Ye M, Sun Q. Ligand displacement-induced fluorescence switch of quantum dots for ultrasensitive detection of cadmium ions. Anal Chim Acta. 2014;812:191–8. https://doi.org/10.1016/j.aca.2014.01.006.
Hung IF-N, Lung K-C, Tso EY-K, Liu R, Chung TW-H, Chu M-Y, et al. Triple combination of interferon beta-1b, lopinavir–ritonavir, and ribavirin in the treatment of patients admitted to hospital with COVID-19: an open-label, randomised, phase 2 trial. Lancet. 2020;395(10238):1695–704. https://doi.org/10.1016/S0140-6736(20)31042-4.
Ich I, editor. Q2 (R1): validation of analytical procedures: text and methodology. Geneva: International conference on harmonization; 2005.
Kanagasubbulakshmi S, Kadirvelu K. Nano interface potential influences in CdTe quantum dots and biolabeling. Appl Nanosci. 2018;8(3):285–95. https://doi.org/10.1007/s13204-018-0774-0.
Kienskaya K, Il'yushenko E, Sardushkin M, Guznova NY, Koldaeva TY, Kusmaev A, et al. Quantitative UV-spectrophotometric determination of ribavirin. Pharm Chem J. 2019;53(2):175–7. https://doi.org/10.1007/s11094-019-01974-5.
Lakowicz JR. Principles of fluorescence spectroscopy. Berlin: Springer; 2006.
Larrat S, Stanke-Labesque F, Plages A, Zarski J-P, Bessard G, Souvignet C. Ribavirin quantification in combination treatment of chronic hepatitis C. Antimicrob Agents Chemother. 2003;47(1):124–9. https://doi.org/10.1128/AAC.47.1.124-129.2003.
Laurent GJ, Shapiro SD. Encyclopedia of respiratory medicine. Cambridge: Academic Press Elsevier; 2006.
Leong CR, Tong WY, Tan W-N, Tumin ND, Yusof FAM, Yacob LS, et al. Synthesis of curcumin quantum dots and their antimicrobial activity on necrotizing fasciitis causing bacteria. Mater Today Proc. 2020;31:31–5. https://doi.org/10.1016/j.matpr.2020.01.082.
Liang Q, Ma W, Shi Y, Li Z, Yang X. Easy synthesis of highly fluorescent carbon quantum dots from gelatin and their luminescent properties and applications. Carbon. 2013;60:421–8. https://doi.org/10.1016/j.carbon.2013.04.055.
Liu R, Yang R, Qu C, Mao H, Hu Y, Li J, et al. Synthesis of glycine-functionalized graphene quantum dots as highly sensitive and selective fluorescent sensor of ascorbic acid in human serum. Sens Actuators B Chem. 2017;241:644–51. https://doi.org/10.1016/j.snb.2016.10.096.
Liu L, Huang Q, Tanveer ZI, Jiang K, Zhang J, Pan H, et al. "Turn off-on" fluorescent sensor based on quantum dots and self-assembled porphyrin for rapid detection of ochratoxin A. Sens Actuators Chem. 2020;302:127212. https://doi.org/10.1016/j.snb.2019.127212.
Mahmoud AM, El-Wekil MM, Mahnashi MH, Ali MF, Alkahtani SA. Modification of N, S co-doped graphene quantum dots with p-aminothiophenol-functionalized gold nanoparticles for molecular imprint-based voltammetric determination of the antiviral drug sofosbuvir. Microchim Acta. 2019;186:1–8. https://doi.org/10.1007/s00604-019-3647-7.
Martin P, Jensen DM. Ribavirin in the treatment of chronic hepatitis C. J Gastroenterol Hepatol. 2008;23(6):844–55. https://doi.org/10.1111/j.1440-1746.2008.05398.x.
Mohamed RM, Mohamed SH, Asran AM, Alsohaimi IH, Hassan HM, Ibrahim H, et al. Bifunctional ratiometric sensor based on highly fluorescent nitrogen and sulfur biomass-derived carbon nanodots fabricated from manufactured dairy product as a precursor. Spectrochim Acta Part A Mol Biomol Spectrosc. 2023;293:122444. https://doi.org/10.1016/j.saa.2023.122444.
Nair A, Haponiuk JT, Thomas S, Gopi S. Natural carbon-based quantum dots and their applications in drug delivery: a review. Biomed Pharmacother. 2020;132:110834. https://doi.org/10.1016/j.biopha.2020.110834.
Pan M, Xie X, Liu K, Yang J, Hong L, Wang S. Fluorescent carbon quantum dots—synthesis, functionalization and sensing application in food analysis. Nanomaterials. 2020;10(5):930. https://doi.org/10.3390/nano10050930.
Parvin N, Mandal TK. Dually emissive P, N-co-doped carbon dots for fluorescent and photoacoustic tissue imaging in living mice. Microchim Acta. 2017;184(4):1117–25. https://doi.org/10.1007/s00604-017-2108-4.
Peng J, Yin W, Shi J, Jin X, Ni G. Magnesium and nitrogen co-doped carbon dots as fluorescent probes for quenchometric determination of paraoxon using pralidoxime as a linker. Microchim Acta. 2019;186(1):1–9. https://doi.org/10.1007/s00604-018-3147-1.
Pharmacopoeia B. British Pharmacopoeia, vol. III. London: Her Majesty's Stationery.
Qi Z-D, Zhou B, Qi X, Chuan S, Liu Y, Dai J. Interaction of rofecoxib with human serum albumin: determination of binding constants and the binding site by spectroscopic methods. J Photochem Photobiol A. 2008;193(2–3):81–8. https://doi.org/10.1016/j.jphotochem.2007.06.011.
Qiang R, Yang S, Hou K, Wang J. Synthesis of carbon quantum dots with green luminescence from potato starch. New J Chem. 2019;43(27):10826–33. https://doi.org/10.1039/C9NJ02291K.
Shahabadi N, Kalar ZM, Vaisi-Raygani A. DNA interaction studies of an antiviral drug, ribavirin, using different instrumental methods. DNA Cell Biol. 2012;31(5):876–82. https://doi.org/10.1089/dna.2011.1456.
Singh G, Kaur H, Sharma A, Singh J, Alajangi HK, Kumar S, et al. Carbon based nanodots in early diagnosis of cancer. Front Chem. 2021;9:669169. https://doi.org/10.3389/fchem.2021.669169.
Snell NJ. Ribavirin-current status of a broad spectrum antiviral agent. Expert Opin Pharmacother. 2001;2(8):1317–24. https://doi.org/10.1517/14656566.2.8.1317.
Thomas E, Ghany MG, Liang TJ. The application and mechanism of action of ribavirin in therapy of hepatitis C. Antivir Chem Chemother. 2012;23(1):1–12. https://doi.org/10.3851/IMP2125.
Uhlenhopp EL, Krasna AI. Denaturation of DNA at pH 7.0 by acid and alkali. Nature. 1969;223(5212):1267–9.
USP30-NF25. United State Pharmacopoeia 30-National Formulary 25. USP; 2007.
Vîjan L, Topală C. Molecular modeling of ribavirin-DNA interaction. Int J Biol Biomed Eng. 2016;10:18–24.
Wadie MA, Mostafa SM, El Adl S, Elgawish MS. Development and validation of a new, simple-HPLC method for simultaneous determination of sofosbuvir, daclatasvir and ribavirin in tablet dosage form. IOSR J Pharm Biol Sci. 2017;12(5):60–8.
Wang C, Sun D, Zhuo K, Zhang H, Wang J. Simple and green synthesis of nitrogen-, sulfur-, and phosphorus-co-doped carbon dots with tunable luminescence properties and sensing application. RSC Adv. 2014;4(96):54060–5. https://doi.org/10.1039/C4RA10885J.
Wang Y, Yue Q, Hu Y, Liu C, Tao L, Zhang C. Synthesis of N-doped carbon dots and application in vanillin detection based on collisional quenching. RSC Adv. 2019;9(69):40222–7. https://doi.org/10.1039/C9RA08352A.
Xiang G, Tong C, Lin H. Nitroaniline isomers interaction with bovine serum albumin and toxicological implications. J Fluoresc. 2007;17:512–21. https://doi.org/10.1007/s10895-007-0203-3.

Youssef AA, Magdy N, Hussein LA, El-Kosasy A. Validated RP-HPLC method for simultaneous determination of ribavirin, sofosbuvir and daclatasvir in human plasma: a treatment protocol administered to HCV patients in Egypt. J Chromatogr Sci. 2019;57(7):636–43. https://doi.org/10.1093/chromsci/bmz038.

Zhang R-p, Zhang Y-n, Zheng X-k, Wang B-b, You J-f. Determination of ribavirin in rat plasma by UPLC-MS/MS: application to a pharmacokinetic study. Lat Am J Pharm. 2016;35(1):118–23.

Zhu S, Meng Q, Wang L, Zhang J, Song Y, Jin H, et al. Highly photoluminescent carbon dots for multicolor patterning, sensors, and bioimaging. Angew Chem. 2013;125(14):4045–9. https://doi.org/10.1002/ange.201300519.

Publisher's Note